Published in final edited form as:
Immunity. 2012 April 20; 36(4): 600–611. doi:10.1016/j.immuni.2012.03.007.

The Adaptor Protein Crk Controls Activation and Inhibition of Natural Killer Cells

Dongfang Liu[1,2], **Mary E. Peterson**[1], and **Eric O. Long**[1,*]

[1]Laboratory of Immunogenetics, National Institute of Allergy and Infectious Diseases, National Institutes of Health, Rockville, MD 20852, USA

SUMMARY

Natural killer (NK) cell inhibitory receptors recruit tyrosine phosphatases to prevent activation, induce phosphorylation and dissociation of the small adaptor Crk from cytoskeleton scaffold complexes, and maintain NK cells in a state of responsiveness to subsequent activation events. How Crk contributes to inhibition is unknown. We imaged primary NK cells over lipid bilayers carrying IgG1 Fc to stimulate CD16, and human leukocyte antigen (HLA)-E to inhibit through receptor CD94-NKG2A. HLA-E alone induced Crk phosphorylation in NKG2A$^+$ NK cells. At activating synapses with Fc alone, Crk was required for the movement of Fc microclusters and their ability to trigger activation signals. At inhibitory synapses, HLA-E promoted central accumulation of both Fc and phosphorylated Crk, and blocked the Fc-induced buildup of F-actin. We propose a unified model for inhibitory receptor function: Crk phosphorylation prevents essential Crk-dependent activation signals and blocks F-actin network formation, thereby reducing constraints on subsequent engagement of activation receptors.

INTRODUCTION

Regulation, both positive and negative, at multiple levels is required to maintain proper balance in cellular responses. Among the mechanisms for negative regulation is the dominant inhibition by receptors that carry immunoreceptor tyrosine-based inhibition motifs (ITIMs) in their cytoplasmic tail (Long, 1999; Ravetch and Lanier, 2000). For example, the cytotoxic activity of natural killer (NK) cells is blocked by the binding of inhibitory receptors to major histocompatibility complex (MHC) class I molecules expressed on target cells (Ciccone et al., 1992; Karlhofer et al., 1992). ITIM-bearing receptors constitute a large family, which are involved in negative regulation of many responses in different types of cells (Daëron et al., 2008; Long, 2008; Ravetch and Lanier, 2000). The importance of understanding the mechanism of inhibition for the purpose of clinical intervention is underscored by the case of exhausted T cells and B cells, which up-regulate expression of multiple ITIM-bearing receptors during chronic viral infection (Barber et al., 2006; Day et al., 2006; Kardava et al., 2011; Virgin et al., 2009).

*Correspondence: eLong@nih.gov.
[2]Present address: Ragon Institute of Massachusetts General Hospital, Massachusetts Institute of Technology and Harvard University, Boston, MA 02114, USA

Supplemental Data
Supplemental data include Supplemental Experimental Procedures, 6 Figures, 7 Movies, and 1 Table.

MHC class I-specific inhibitory receptors have a role in promoting intrinsic responsiveness of NK cells to subsequent activation signals (i.e. signals delivered in the absence of inhibitory receptor engagement) (Anfossi et al., 2006; Hoglund and Brodin, 2010; Kim et al., 2005). NK cells tune their responsiveness commensurate with the strength of signals received from inhibitory receptors (Brodin et al., 2009; Hoglund and Brodin, 2010; Joncker et al., 2009). However, it is not clear yet whether inhibitory receptors prevent desensitization of NK cells caused by continuous stimulation, the "disarming" model, and/or deliver a specific signal that results in "arming" or "licensing" of NK cells (Joncker and Raulet, 2008; Yokoyama and Kim, 2006).

Inhibitory receptors on NK cells have been the prototype in studies of the ITIM-based inhibitory signaling pathway (Burshtyn and Long, 1997; Daëron et al., 2008; Long, 2008). In human NK cells, they include the family of killer cell Ig-like receptors (KIR) and the lectin-like heterodimer CD94-NKG2A. Phosphorylation of two ITIMs in the cytoplasmic tail of an inhibitory receptor results in specific recruitment of tyrosine phosphatase SHP-1, or SHP-2 (Burshtyn et al., 1996; Olcese et al., 1996). SHP-1 is required for ITIM-dependent functional inhibition of natural cytotoxicity (Burshtyn et al., 1996; Gupta et al., 1997). Work on some of the other members of the ITIM-bearing receptor family suggests a similar mechanism for inhibition (Daëron et al., 2008; Long, 2008). An advance in understanding inhibitory signaling was the identification of Vav1 as a major substrate of SHP-1 in NK cells during inhibition by MHC class I on target cells (Peterson and Long, 2008; Stebbins et al., 2003). Given the essential role of Vav1 in TCR-dependent signals for Ca^{2+} mobilization, F-actin remodeling, and synapse formation (Tybulewicz, 2005), dephosphorylation of the activating phospho-tyrosines in Vav1 can explain the inhibition of actin-dependent signals by ITIM-bearing receptors (Dietrich et al., 2001; Guerra et al., 2002; Masilamani et al., 2006; Riteau et al., 2003).

A new component of the inhibitory signaling pathway used by KIR and by CD94-NKG2A has been identified (Peterson and Long, 2008). During contact of NK cells with target cells that express an MHC class I ligand for the inhibitory receptor, the small adaptor Crk becomes phosphorylated, associates with the tyrosine kinase c-Abl, and dissociates from signaling complexes that form during activation. A membrane-targeted form of Crk lacking the tyrosine that serves as substrate for c-Abl can partially overcome inhibition by KIR, suggesting that phosphorylation of Crk contributes to inhibition (Peterson and Long, 2008). Complexes of Crk with the scaffold proteins c-Cbl and p130CAS contribute to cytoskeletal organization and promote actin-driven lamellipodiae (Birge et al., 2009; Chodniewicz and Klemke, 2004; Nakashima et al., 1999). There are two isoforms of Crk, CrkII and CrkL, which are encoded by separate genes (Matsuda et al., 1992; ten Hoeve et al., 1993). Each is composed of one Src homology-2 (SH2) and two SH3 domains. NK cells express both isoforms, which we refer to here as Crk. Crk binds to phosphorylated tyrosine motifs in p130CAS and c-Cbl via its SH2 domain, and recruits the guanine exchange factor C3G via the N-terminal SH3 domain. C3G activates the small GTPase Rap1, which promotes leukocyte function-associated antigen-1 (LFA-1)–dependent adhesion (Reedquist et al., 2000). The phosphorylation of Crk during inhibition of NK cells has raised new questions about the role of Crk in NK cell activation, the contribution of Crk phosphorylation to inhibition, and how it may relate to the ITIM-dependent tuning of NK cell responsiveness.

To address these questions, we imaged human primary NK cells over supported planar lipid bilayers that carry ligands of activating and inhibitory receptors. Live imaging would provide information on the dynamics of inhibitory immunological synapses not available from previous images of fixed NK cells (Almeida and Davis, 2006; Culley et al., 2009; Davis et al., 1999; Vyas et al., 2001). Inhibitory synapses were formed with the combination of an IgG1 Fc as a ligand for CD16 and of HLA-E as a ligand for inhibitory receptor CD94-

NKG2A. Our live imaging showed that both ligands coalesced into a single central cluster at the early phase of inhibitory synapse formation. HLA-E inhibited the formation of Fc microclusters, but not the central accumulation of Fc. Crk was phosphorylated in response to CD94-NKG2A binding to HLA-E, and accumulated at the center of inhibitory synapses. Silencing of Crk expression in primary NK cells resulted in impaired activation through CD16, as shown by deficient Fc clustering and decreased Vav1 phosphorylation. Crk silencing also impaired the ability of inhibitory receptors to prevent central accumulation of F-actin. A model for ITIM-based inhibition is proposed to accommodate these findings.

RESULTS

Inhibitory Immunological Synapses with Primary NK Cells

To image inhibitory immunological synapses, we used human primary NK cells over lipid bilayers carrying ligands for activating and inhibitory receptors. For activation, human IgG1 Fc was used to engage FcγRØ (CD16). HLA-E is a ligand for both inhibitory CD94-NKG2A and activating CD94-NKG2C receptors. We therefore depleted NKG2C$^+$ NK cells from our NK cell preparations (Figure S1). The distribution of Fc alone and of HLA-E alone was imaged by 3-dimensional (3D) confocal microscopy and 2-dimensional (2D) total internal reflection fluorescence (TIRF) microscopy. Images of fixed NK cells showed that Fc and HLA-E accumulated at the center of synapses (Figure 1A, 1B, and 1C). About 65% of HLA-E clusters included a central hole (Figure 1D). Lipid bilayers carrying both Fc and HLA-E were used to image inhibitory synapses. As NKG2A is expressed on a subset of primary NK cells, we used clustering of HLA-E as our operational definition of inhibitory synapses. We imaged degranulation on live cells, as described (Liu et al., 2009), to monitor inhibition. Consistent with dominant inhibition of CD16 by CD94-NKG2A (Bryceson et al., 2009), NKG2A$^+$ NK cells did not degranulate, while strong degranulation occurred in NK cells that did not engage HLA-E (Movie S1).

As shown by 3D confocal microscopy, Fc was observed mostly at the center, surrounded by HLA-E (Figure 1E). This organized pattern was also observed with live NK cells in 2D TIRF images (Figure 1F and Movie S2). The majority of inhibitory synapses appeared well-organized (Figure 1G). Therefore, primary NK cells form inhibitory synapses over lipid bilayers carrying ligands for CD16 and CD94-NKG2A.

On lipid bilayers carrying Fc alone, Fc formed peripheral microclusters, which moved toward the center, where they accumulated (Figure 2A and Movie S3). HLA-E alone also accumulated rapidly at the center, apparently by forming a peripheral ring that moved toward the center (Figure 2B and Movie S4). Live images of inhibitory synapses formed over Fc and HLA-E revealed dynamics that could not have been inferred from images of fixed cells. Fc and HLA-E formed a few transient microclusters (Figure 2C and Movie S5) and converged to form a single central cluster (Figure 2C). The number of Fc clusters formed in the presence of HLA-E was reduced (7 ± 1.2), as compared to the number observed with Fc alone (15 ± 2.3) (Figure 2D). However, the size of central Fc clusters was not affected by HLA-E (Figure 2E). We conclude that inhibitory receptor CD94-NKG2A blocks the formation of Fc microclusters, but not the overall accumulation of Fc at the center of inhibitory synapses.

HLA-E Induces Crk Phosphorylation in NKG2A$^+$ NK Cells

Binding of inhibitory NK cell receptors to MHC class I on target cells induces tyrosine phosphorylation of the adaptor Crk, concomitant with dephosphorylation of Vav1 (Peterson and Long, 2008). To examine these signaling events, we fixed and stained NK cells on lipid bilayers with phosphospecific Abs to Vav1 and Crk. Phosphorylation of Vav1 at tyrosine

174 (pY174-Vav1) is a marker of activation. The majority of NK cells activated by Fc showed strong staining for pY174-Vav1, which had a fair overlap with the Fc cluster under 3D reconstructions of confocal slices (Figure 3A). Most of the synapses formed with HLA-E alone did not show any central pY174-Vav1 staining (Figure 3B). However, punctate staining for pY174-Vav1 was often observed at the edge of NK cells (Figure 3B), which may relate to active peripheral membrane dynamics. Phosphorylation of Crk was examined with an Ab to CrkL phosphorylated at tyrosine 207 (pY207-CrkL). No pY207-CrkL was seen at activating synapses induced by Fc alone (Figure 3C). In contrast, central pY207-CrkL staining was obtained with NK cells bound to HLA-E (Figure 3D). There was very good overlap between pY207-CrkL staining and the HLA-E cluster. These results suggest that engagement of CD94-NKG2A by HLA-E alone is sufficient to induce Crk phosphorylation.

We considered the possibility that HLA-E, which was refolded with β2-microglobulin and peptide after expression in bacteria, could induce Crk phosphorylation independently of its binding to NKG2A. A control experiment using $NKG2C^+$ NK cells (obtained by depletion of $NKG2A^+$ cells) was devised to directly test it. HLA-E clusters formed with $NKG2C^+$ NK cells, but did not show staining for pY207-CrkL (Figure S2). Therefore, Crk phosphorylation occurs only when HLA-E bound to the inhibitory receptor CD94-NKG2A. To further demonstrate Crk phosphorylation in NK cells bound to HLA-E alone and to visualize Crk phosphorylation in live cells, primary NK cells expanded in interleukin-2 (IL-2) were transfected with a CrkL biosensor, which includes a truncated CrkL protein sandwiched between Venus, a variant of YFP, and enhanced cyan fluorescent proteins (Mizutani et al., 2010). The CrkL biosensor is designed to emit Förster resonance energy transfer (FRET) signals when CrkL is phosphorylated (Mizutani et al., 2010). As control, we generated a mutant in which tyrosine 207 had been changed to phenylalanine (Y207F). A strong signal, measured as the ratio of FRET and ECFP emissions, was observed in NK cells bound to HLA-E (Figure S3). Crk phosphorylation was highly dynamic, suggesting a continuous balance of phosphorylation and dephosphorylation (Movie S6). These results confirm that HLA-E alone induces phosphorylation of Crk in $NKG2A^+$ NK cells.

We then stained fixed NK cells that had formed inhibitory synapses over lipid bilayers carrying Fc and HLA-E. pY174-Vav1 was detected at the center of most inhibitory synapses (Figure 3E), but a quantitative analysis by TIRF microscopy showed that the fluorescence intensity of pY174-Vav1 was lower than it was in NK cells stimulated by Fc alone (Figure 3F), consistent with dephosphorylation of Vav1 by SHP-1 during inhibition of NK cells (Peterson and Long, 2008; Stebbins et al., 2003). Staining for pY207-CrkL in fixed inhibitory synapses formed over Fc and HLA-E revealed strong accumulation of phosphorylated Crk at the center of inhibitory synapses (Figure 3G). Tracings of fluorescence intensity of HLA-E and pY207-CrkL across several inhibitory synapses showed that p-CrkL was distributed mostly inside a ring of HLA-E (Figure S4). These images cannot determine where CrkL becomes phosphorylated, i.e. whether it was phosphorylated at the center of the synapse or whether phosphorylated CrkL moved to the center. Note, however, that Fc and HLA-E overlapped at the early stages of inhibitory synapse formation (Figure 2C). A quantitative analysis of TIRF images showed that the intensity of phosphorylated Crk was even higher than on lipid bilayer carrying HLA-E only (Figure 3H). Therefore, we conclude that central accumulation of phosphorylated Crk is a striking feature of inhibitory synapses formed by $NKG2A^+$ NK cells over Fc and HLA-E.

We next tested whether the accumulation of phosphorylated Crk occurred also at inhibitory synapses of NK cells in contact with a target cell. Tyrosine phosphorylation of Crk has been detected after the binding of NK cells to resistant, HLA-class I expressing target cells (Peterson and Long, 2008). The $NKG2A^+$ cell line NKL cell was allowed to form

conjugates with the HLA class I-negative cell line 721.221 and 721.221 cells expressing HLA-E at the cell surface (221-E). As expected, phosphorylated Vav1 accumulated at synapses of NKL with 721.221 cells, but not at inhibitory synapses with 221-E cells (Figure 4). Perforin-containing lytic granules polarized toward 721.221 cells, but not 221-E cells (Figure 4). In contrast, phosphorylated Crk was not detected at activating synapses, but accumulated at inhibitory synapses of NKL with 221-E cells (Figure 4). Thus, the presence of phosphorylated Crk is a general feature of inhibitory synapses formed between NK cells and membranes that include a ligand for an MHC class I-specific inhibitory receptor on the NK cells.

Impaired Fc Clustering and Vav1 Phosphorylation after Crk Silencing

To investigate the role of Crk in activating synapse formation and signaling, expression of CrkII and CrkL was silenced in NKG2C^{+}-depleted, IL-2–activated NK cells by siRNA transfection (Figure S5). After Crk silencing, NK cells on lipid bilayers carrying Fc displayed Fc clusters that remained dispersed over the entire synapse and failed to move toward the center (Figure 5A, 5B, and Movie S7). To overcome the partial Crk silencing by siRNA (Figure S5), we stained the fixed cells with an Ab to CrkL and selected cells with strong Crk silencing to image pY174-Vav1. Staining for pY174-Vav1 revealed a striking decrease after Crk silencing, as seen by TIRF microscopy (Figure 5B) and 3D confocal imaging (Figure 5C). A quantitative analysis of TIRF images showed that the intensity of p-Vav1 in Crk-silenced NK cells was decreased (Figure 5D). We conclude that Crk controls not only the clustering of activating receptors, but also their ability to signal.

Despite incomplete Crk silencing in the NK cell population (Figure S5) degranulation by NK cells stimulated with an Ab to CD16 was reduced by 19.2% ± 9.6% (n = 9, $p = 0.0003$), as compared to NK cells transfected with control siRNA (Table S1). These results are in line with other studies (Peterson and Long, 2008; Segovis et al., 2009) and show that Crk (either CrkII, CrkL, or both) contributes to CD16-induced degranulation.

HLA-E Restores Fc Clustering after Crk Silencing

Clustering of HLA-E on lipid bilayers was not affected by Crk silencing, as seen by TIRF microscopy with live (Figure 6A) and fixed (Figure 6B) NK cells. Similar results were obtained by 3D confocal microscopy (Figure 6C). We then examined inhibitory synapses formed with Fc and HLA-E. By TIRF microscopy, Fc, HLA-E and pY207-CrkL all appeared accumulated at the center of the inhibitory synapse (Figure 6D). This synapse was probably caught at an earlier stage than inhibitory synapses where Fc and HLA-E have been segregated (as in Figure 3G). A strong co-localization of Fc and HLA-E was also observed after Crk silencing (Figure 6D), even though Crk silencing impaired the clustering of Fc alone (Figure 5). Therefore, HLA-E overcomes the Crk-dependence of Fc clustering and promotes Fc clustering in the absence of Crk.

The ability of HLA-E to cluster and to promote clustering of Fc may be related to the role of the actin cytoskeleton in receptor movement. Clustering and signaling by most transmembrane receptors at the cell surface requires actin polymerization. One exception is the clustering of inhibitory KIR upon binding to HLA-C, which is not completely dependent on actin polymerization (Davis et al., 1999; Faure et al., 2003; Standeven et al., 2004). To understand how F-actin may contribute to receptor clustering and inhibitory synapse formation, we tested the effect of cytochalasin D (Cyto D) on activating and inhibitory synapses. A short incubation of 2 to 5 minutes with low concentrations of Cyto D (0.5 or 1.0 μM) was used. After Cyto D treatment, primary NK cells were tested on lipid bilayers carrying Fc: Clustering of Fc was undetectable by 3D confocal (Figure S6A) and 2D TIRF microscopy (Figure S6B). In contrast, HLA-E clustering was observed with NK cells added

to lipid bilayers carrying HLA-E alone after Cyto D treatment (Figure S6C and S6D). Furthermore, clusters of Fc were observed after Cyto D treatment of NK cells on lipid bilayers carrying Fc and HLA-E (Figure S6E and S6F). These results show that CD94-NKG2A promotes clustering of CD16 by overcoming the need for actin polymerization in CD16 clustering. They further suggest that the Crk-dependence of CD16 clustering is due to the contribution of Crk to actin dynamics.

Crk Is Required for HLA-E–Dependent Control of F-Actin Remodeling

To further address how Crk controls immunological synapse formation, we imaged F-actin in NK cells over lipid bilayers. NK cells have little basal F-actin, which appeared evenly dispersed in both control NK cells and NK cells after Crk silencing (Figure 7A). At activating synapses formed with Fc alone, accumulation of F-actin was clearly observed in the central part of the synapse, but extending further to the periphery than the Fc cluster (Figure 7B). After Crk silencing, dispersed Fc clusters were observed, as in Figure 5, but actin remodeling was impaired, as F-actin appeared as disorganized patches (Figure 7B). In NK cells bound to HLA-E alone, F-actin did not accumulate at the center but formed a peripheral ring (Figure 7C). HLA-E clustering still occurred after Crk silencing, but F-actin was more evenly distributed than in control cells (Figure 7C). At inhibitory synapses formed over Fc and HLA-E, F-actin accumulated only at the cell periphery, and HLA-E formed a concentric ring inside the F-actin region (Figure 7D). These results suggest that the phosphorylation of Crk at the center of inhibitory synapses prevents F-actin accumulation. Furthermore, F-actin appeared at the center of inhibitory synapses after Crk silencing (Figure 7D). We conclude that Crk-dependent signaling by inhibitory receptor CD94-NKG2A prevents F-actin accumulation in the central region of inhibitory synapses.

DISCUSSION

Activation of many types of cellular responses is under negative control by ITIM-bearing receptors (Long, 2008). A common feature among receptors in the large ITIM-receptor family is recruitment of tyrosine phosphatases SHP-1 and SHP-2, which block tyrosine kinase-dependent activation pathways. However, we have shown here that dephosphorylation by SHP phosphatases was not the only component contributing to inhibition. We have imaged inhibitory immunological synapses formed by primary $NKG2A^+$ NK cells over lipid bilayers carrying ligands for activation (CD16) and inhibition (CD94-NKG2A) receptors. Binding of inhibitory receptor to HLA-E blocked the formation of IgG1 Fc microclusters, but not the central accumulation of IgG1 Fc at inhibitory synapses. HLA-E was sufficient to induce phosphorylation of Crk in $NKG2A^+$ NK cells. Silencing experiments with siRNA showed that Crk was required for IgG1 Fc microcluster movement and Vav1 phosphorylation during activation, and for the block in F-actin accumulation during inhibition. Our findings support a revised model for inhibition: Phosphorylation of adaptor Crk induced by inhibitory receptors blocks essential, Crk-dependent signaling for NK cell activation.

The minimal requirements to form an inhibitory NK cell synapse is to activate through CD16, which induces degranulation, and inhibit through an ITIM-bearing receptor like CD94-NKG2A, as shown with an insect cell line transfected with HLA-E (Bryceson et al., 2009). We have reconstituted these receptor–ligand interactions by attaching IgG1 Fc and HLA-E onto lipid bilayers. The live images obtained here have given insights into the inhibitory mechanism, which had not been apparent from images of fixed NK cell immunological synapses. The concentric distribution of activating receptors at the center surrounded by inhibitory receptors was typical of mature synapses. In contrast, early events, which are more likely to correspond to active signaling events, were highly dynamic. Addition of HLA-E to IgG1 Fc on the lipid bilayer reduced the number of Fc microclusters,

as compared to clusters formed with Fc alone. As TCR and BCR microclusters that migrate from the periphery of cells to the center of immunological synapses represent active signaling platforms (Harwood and Batista, 2010; Tolar et al., 2008; Varma et al., 2006), it is likely that peripheral Fc microclusters contribute to NK cell activation.

The primary NK cells used here formed stable inhibitory synapses, unlike the cell line NKL transfected with KIR2DL2 on lipid bilayers carrying ULBP3 (a ligand for activating receptor NKG2D) and HLA-Cw3 (a ligand for inhibitory receptor KIR2DL2) (Abeyweera et al., 2011). To overcome the weak inhibitory synapse formation by NKL cells, Huse's group used a photoactivation system to switch inhibition on after NKL cells had already formed an activating synapse. Photoactivation of HLA-Cw3 results in rapid formation of HLA-C microclusters at the cell periphery and a concomitant loss of the formation of new ULBP3 microclusters (Abeyweera et al., 2011). Our results are consistent with theirs in one important aspect: HLA-E engagement impaired the formation of Fc microclusters. Therefore, inhibition of CD16 by CD94-NKG2A is similar to inhibition of NKG2D signals by KIR2DL2. However, we also observed the formation of a large central co-cluster of Fc with HLA-E. Our data shows that inhibitory receptors block the ability of activation receptors to signal rather than their accumulation at the synapse. These results are consistent with our earlier work showing that binding of inhibitory KIR to HLA-C promotes the clustering of activation receptors 2B4 and CD2 (Schleinitz et al., 2008).

HLA-E alone on the lipid bilayer was sufficient to induce phosphorylation of Crk, as detected with a phospho-specific Ab in fixed cells, and with a FRET biosensor in live cells. Phosphorylated Crk was also detected at inhibitory synapses formed with human target cells that express HLA-E. The ability of CD94-NKG2A to induce a phosphorylation event in the absence of other receptor–ligand interactions represents a paradigm shift for signaling by an ITIM-bearing receptor. It should no longer be considered a co-inhibition receptor that signals only in the context of signaling by activation receptors.

Silencing of Crk expression with siRNAs targeted to both isoforms, CrkII and CrkL, had profound effects on NK cell activation by IgG1 Fc. Movement of Fc microclusters, phosphorylation of Vav1, and accumulation of F-actin were all greatly reduced. This result places Crk at a very proximal step of the activation pathway, upstream of the bulk of Vav1 phosphorylation. In contrast, HLA-E clustering was not affected by Crk silencing, and could in fact restore Fc clustering. Even though HLA-E clustering occurred after Crk silencing, Crk was required for the ability of HLA-E to prevent accumulation of F-actin at inhibitory synapses. It is likely that F-actin is disrupted through Crk phosphorylation, which causes disassembly of Crk from scaffold proteins p130CAS and c-Cbl and from the guanine exchange factor C3G.

The outcome of Crk phosphorylation during inhibition was not equivalent to an absence of Crk, as obtained after Crk silencing. Central accumulation of IgG1 Fc was unimpeded during inhibition but was blocked in the absence of Crk. The possibility that sufficient functional, unphosphorylated Crk remained during inhibition to promote F-actin-dependent clustering is unlikely because central Fc accumulation was resistant to cytochalasin D and occurred in a zone that appeared to be depleted of F-actin. The unusual property of inhibitory receptors of promoting actin-independent clustering of activation receptors may be related to Crk phosphorylation. Phosphorylated Crk could even play a direct role, in addition to the fact that it has been dissociated from signaling complexes. Phosphorylation provides much finer temporal and spatial regulation than the presence or absence of a molecule: Local Crk phosphorylation may disrupt F-actin at the center of inhibitory synapses, while allowing formation of a peripheral F-actin ring.

We propose a model for inhibitory signaling that incorporates the important contribution of regulation by Crk, and how it could account for the ITIM-dependent maintenance of NK cell responsiveness to subsequent activation (also known as NK cell licensing). The model is still compatible with an important contribution of SHP-1 to inhibition. It is clear that the underlying actin network is essential for the formation of, and signaling by microclusters of activation receptors. As an efficient way to block NK cell activation at a proximal step, even upstream of Vav1 phosphorylation, inhibitory receptors disrupt the actin network through phosphorylation of Crk. This model can explain the reduction in newly formed microclusters of activating receptors when inhibitory receptors are engaged. Inhibitory receptors may exploit the properties of Crk to achieve their dual function, i.e. inhibition and NK cell licensing. For inhibition, they block activation by inducing Crk phosphorylation to prevent actin-dependent signaling. But, somewhat counterintuitively, Crk phosphorylation may also set the stage for a more efficient activation receptor engagement (once inhibition has been removed) by reducing the constraints imposed by the F-actin network on receptor movement.

A recent study has reported that activation receptors NK1.1 and NKp46 on mouse NK cells display a more constrained movement at the plasma membrane in mice that lacked MHC class I ligands for inhibitory receptors (Guia et al., 2011). Evidence was provided that NKp46 movement on these hyporesponsive NK cells is confined by an actin-based meshwork (Guia et al., 2011). We propose that greater lateral mobility of activation receptors, due to Crk phosphorylation in licensed NK cells, may endow them with enhanced signaling capacity once inhibition is removed. According to this model, licenses would expire quickly, consistent with an NK cell responsiveness that is easily tuned according to the MHC class I environment (Hoglund and Brodin, 2010). Although our model supports the “licensing” hypothesis (Kim et al., 2005), it does not exclude a loss of responsiveness or “disarming” of NK cells that are stimulated repeatedly in the absence of inhibition (Joncker and Raulet, 2008).

As Crk phosphorylation occurred after binding of two structurally distinct inhibitory receptors, CD94-NKG2A and KIR2DL1, to their MHC class I ligands on human target cells (Peterson and Long, 2008), the model for ITIM-dependent inhibition through Crk phosphorylation described here is likely to be relevant to many other cellular responses controlled by receptors in the large ITIM family.

EXPERIMENTAL PROCEDURES

Cells

NK cells were isolated from human peripheral blood by negative selection (Stem Cell Technologies, Vancouver, BC), and were > 99% $CD3^{-}CD56^{+}$. Human blood samples from anonymized healthy donors were drawn for research purposes at the NIH Blood Bank under an NIH IRB approved protocol with informed consent. Freshly isolated NK cells were resuspended in Iscove’s modified Dulbecco medium (IMDM; Mediatech, Manassas, VA) supplemented with 10% human serum (Valley Biomedical, Winchester, VA) without IL-2, and were used within 2 days. IL-2–activated NK cells were cultured in OpTmizer (Invitrogen) supplemented with 10% purified IL-2 (Hemagen), 100 units/ml recombinant IL-2 (Roche) and 5 μg/ml phytohemaglutinin (PHA, Sigma), and expanded in the same medium without PHA and feeder cells, as described (March and Long, 2011). To remove $NKG2C^{+}$ or $NKG2A^{+}$ NK cells, anti-NKG2C (Clone 134522, R&D Systems) or anti-NKG2A (Z199, Beckman Coulter) was added to NK cells, followed by biotinylated Rat anti-mouse IgG2b antibody (R12-3, BD Pharmingen) and anti-biotin microbeads (Miltenyi Biotec, Auburn, CA), and depleted using an LS column (Miltenyi Biotec, Auburn, CA). The human cell line NKL (a gift of M. Robertson) was cultured in RPMI 1640 (Mediatech,

Manassas VA) containing 10% fetal calf serum, 2 mM L-glutamine (Invitrogen), 1 mM sodium pyruvate (Invitrogen), and 100 U/ml of recombinant IL-2 (Hoffmann-La Roche). The 721.221 cell transfected with HLA-E (221-AEH) was a gift of D. Geraghty (Fred Hutchison Cancer Research Center, Seattle).

Antibodies and Reagents

The pY207-CrkL and pY174-Vav1 Abs were from Cell Signaling Technology Inc. (Danvers, MA) and Abcam (Cambridge, MA), respectively. The specificity and selectivity of pY207-CrkL and pY174-Vav1 antibodies was evaluated by immuno-blotting lysates of primary NK cells that had been treated with 4 mM $NaVO_4$. Other Abs and their source were: perforin mAb (δG9, Pierce Chemical Co.), anti-NKG2A mAb (Z199, Beckman Coulter, Fullerton, CA), anti-NKG2C mAb (134522, R&D Systems, Minneapolis, MN); Alexa Fluor 488-, 568-, and 647-labeled isotype-specific goat anti-mouse Abs (Molecular Probes Inc., Eugene, OR). For cytochalasin D inhibition, NK cells were pre-incubated with 0.5 or 1.0 μM cytochalasin D (BIOMOL International L.P., PA) for 1 to 2 min at 37°C before adding onto bilayers. The 1, 2-Dioleoyl-sn-Glycero-3-Phosphocholine (DOPC) and 1, 2-Dioleoyl-sn-Glycero-3-[(N-(5-amino-1-carboxypentyl) iminodiacetic acid) succinyl] (Nickel salt) (DOGS-NTA) were from Avanti Polar Lipids, Inc (Alabaster, AL). A CrkL biosensor plasmid, called Pickles2.31 (Mizutani et al., 2010), was a gift of Yusuke Ohba (Hokkaido University Graduate School of Medicine, Sapporo, Japan). The CrkL tyrosine at amino acid 207 in Pickles 2.31 was mutated to phenylalanine using Quick Change Mutagenesis (Stratagene, LaJolla, CA). The following primers were used: Forward (5′-GAACCTGCTCATGCATTTGCTCAACCTCAGACC-3′) and Reverse (5′-GGTCTGAGGTTGAGCAAATGCATGAGCAGGTTC-3′). The mutation was confirmed by sequencing.

Supplementary Material

Refer to Web version on PubMed Central for supplementary material.

Acknowledgments

We thank J. Brzostowski, S. Rajagopalan, and P. Sun for advice and help, D. Geraghty and M. Robertson for cell lines, and Y. Ohba for the CrkL biosensor. This work has been supported by the Intramural Research Program of the National Institutes of Health, National Institute of Allergy and Infectious Diseases.

References

Abeyweera TP, Merino E, Huse M. Inhibitory signaling blocks activating receptor clustering and induces cytoskeletal retraction in natural killer cells. J Cell Biol. 2011; 192:675–690. [PubMed: 21339333]

Almeida CR, Davis DM. Segregation of HLA-C from ICAM-1 at NK cell immune synapses is controlled by its cell surface density. J Immunol. 2006; 177:6904–6910. [PubMed: 17082605]

Anfossi N, Andre P, Guia S, Falk CS, Roetynck S, Stewart CA, Breso V, Frassati C, Reviron D, Middleton D, et al. Human NK cell education by inhibitory receptors for MHC class I. Immunity. 2006; 25:331–342. [PubMed: 16901727]

Barber DL, Wherry EJ, Masopust D, Zhu B, Allison JP, Sharpe AH, Freeman GJ, Ahmed R. Restoring function in exhausted CD8 T cells during chronic viral infection. Nature. 2006; 439:682–687. [PubMed: 16382236]

Birge RB, Kalodimos C, Inagaki F, Tanaka S. Crk and CrkL adaptor proteins: networks for physiological and pathological signaling. Cell Commun Signal. 2009; 7:13. [PubMed: 19426560]

Brodin P, Karre K, Hoglund P. NK cell education: not an on-off switch but a tunable rheostat. Trends Immunol. 2009; 30:143–149. [PubMed: 19282243]

Bryceson YT, Ljunggren HG, Long EO. Minimal requirement for induction of natural cytotoxicity and intersection of activation signals by inhibitory receptors. Blood. 2009; 114:2657–2666. [PubMed: 19628705]

Burshtyn DN, Long EO. Regulation through inhibitory receptors: lessons from natural killer cells. Trends Cell Biol. 1997; 7:473–479. [PubMed: 17709010]

Burshtyn DN, Scharenberg AM, Wagtmann N, Rajagopalan S, Berrada K, Yi T, Kinet JP, Long EO. Recruitment of tyrosine phosphatase HCP by the killer cell inhibitor receptor. Immunity. 1996; 4:77–85. [PubMed: 8574854]

Chodniewicz D, Klemke RL. Regulation of integrin-mediated cellular responses through assembly of a CAS/Crk scaffold. Biochim Biophys Acta. 2004; 1692:63–76. [PubMed: 15246680]

Ciccone E, Pende D, Viale O, Than A, Di Donato C, Orengo AM, Biassoni R, Verdiani S, Amoroso A, Moretta A, Moretta L. Involvement of HLA class I alleles in natural killer (NK) cell-specific functions: expression of HLA-Cw3 confers selective protection from lysis by alloreactive NK clones displaying a defined specificity (specificity 2). J Exp Med. 1992; 176:963–971. [PubMed: 1328466]

Culley FJ, Johnson M, Evans JH, Kumar S, Crilly R, Casasbuenas J, Schnyder T, Mehrabi M, Deonarain MP, Ushakov DS, et al. Natural killer cell signal integration balances synapse symmetry and migration. PLoS Biol. 2009; 7:e1000159. [PubMed: 19636352]

Daëron M, Jaeger S, Du Pasquier L, Vivier E. Immunoreceptor tyrosine-based inhibition motifs: a quest in the past and future. Immunol Rev. 2008; 224:11–43. [PubMed: 18759918]

Davis DM, Chiu I, Fassett M, Cohen GB, Mandelboim O, Strominger JL. The human natural killer cell immune synapse. Proc Natl Acad Sci USA. 1999; 96:15062–15067. [PubMed: 10611338]

Day CL, Kaufmann DE, Kiepiela P, Brown JA, Moodley ES, Reddy S, Mackey EW, Miller JD, Leslie AJ, DePierres C, et al. PD-1 expression on HIV-specific T cells is associated with T-cell exhaustion and disease progression. Nature. 2006; 443:350–354. [PubMed: 16921384]

Dietrich J, Cella M, Colonna M. Ig-like transcript 2 (ILT2)/leukocyte Ig-like receptor 1 (LIR1) inhibits TCR signaling and actin cytoskeleton reorganization. J Immunol. 2001; 166:2514–2521. [PubMed: 11160312]

Faure M, Barber DF, Takahashi SM, Jin T, Long EO. Spontaneous clustering and tyrosine phosphorylation of NK cell inhibitory receptor induced by ligand binding. J Immunol. 2003; 170:6107–6114. [PubMed: 12794140]

Guerra N, Michel F, Gati A, Gaudin C, Mishal Z, Escudier B, Acuto O, Chouaib S, Caignard A. Engagement of the inhibitory receptor CD158a interrupts TCR signaling, preventing dynamic membrane reorganization in CTL/tumor cell interaction. Blood. 2002; 100:2874–2881. [PubMed: 12351398]

Guia S, Jaeger BN, Piatek S, Mailfert S, Trombik T, Fenis A, Chevrier N, Walzer T, Kerdiles YM, Marguet D, et al. Confinement of activating receptors at the plasma membrane controls natural killer cell tolerance. Sci Signal. 2011; 4:ra21. [PubMed: 21467299]

Gupta N, Scharenberg AM, Burshtyn DN, Wagtmann N, Lioubin MN, Rohrschneider LR, Kinet JP, Long EO. Negative signaling pathways of the killer cell inhibitory receptor and FcgammaRIIb1 require distinct phosphatases. J Exp Med. 1997; 186:473–478. [PubMed: 9236201]

Harwood NE, Batista FD. Early events in B cell activation. Annu Rev Immunol. 2010; 28:185–210. [PubMed: 20192804]

Hoglund P, Brodin P. Current perspectives of natural killer cell education by MHC class I molecules. Nat Rev Immunol. 2010; 10:724–734. [PubMed: 20818413]

Joncker NT, Fernandez NC, Treiner E, Vivier E, Raulet DH. NK cell responsiveness is tuned commensurate with the number of inhibitory receptors for self-MHC class I: the rheostat model. J Immunol. 2009; 182:4572–4580. [PubMed: 19342631]

Joncker NT, Raulet DH. Regulation of NK cell responsiveness to achieve self-tolerance and maximal responses to diseased target cells. Immunol Rev. 2008; 224:85–97. [PubMed: 18759922]

Kardava L, Moir S, Wang W, Ho J, Buckner CM, Posada JG, O'Shea MA, Roby G, Chen J, Sohn HW, et al. Attenuation of HIV-associated human B cell exhaustion by siRNA downregulation of inhibitory receptors. J Clin Invest. 2011; 121:2614–2624. [PubMed: 21633172]

Karlhofer FM, Ribaudo RK, Yokoyama WM. MHC class I alloantigen specificity of Ly-49+ IL-2-activated natural killer cells. Nature. 1992; 358:66–70. [PubMed: 1614533]

Kim S, Poursine-Laurent J, Truscott SM, Lybarger L, Song YJ, Yang LP, French AR, Sunwoo JB, Lemieux S, Hansen TH, Yokoyama WM. Licensing of natural killer cells by host major histocompatibility complex class I molecules. Nature. 2005; 436:709–713. [PubMed: 16079848]

Liu D, Bryceson YT, Meckel T, Vasiliver-Shamis G, Dustin ML, Long EO. Integrin-dependent organization and bidirectional vesicular traffic at cytotoxic immune synapses. Immunity. 2009; 31:99–109. [PubMed: 19592272]

Long EO. Regulation of immune responses through inhibitory receptors. Annu Rev Immunol. 1999; 17:875–904. [PubMed: 10358776]

Long EO. Negative signaling by inhibitory receptors: the NK cell paradigm. Immunol Rev. 2008; 224:70–84. [PubMed: 18759921]

March ME, Long EO. beta2 integrin induces TCRzeta-Syk-phospholipase C-gamma phosphorylation and paxillin-dependent granule polarization in human NK cells. J Immunol. 2011; 186:2998–3005. [PubMed: 21270398]

Masilamani M, Nguyen C, Kabat J, Borrego F, Coligan JE. CD94/NKG2A inhibits NK cell activation by disrupting the actin network at the immunological synapse. J Immunol. 2006; 177:3590–3596. [PubMed: 16951318]

Matsuda M, Tanaka S, Nagata S, Kojima A, Kurata T, Shibuya M. Two species of human CRK cDNA encode proteins with distinct biological activities. Mol Cell Biol. 1992; 12:3482–3489. [PubMed: 1630456]

Mizutani T, Kondo T, Darmanin S, Tsuda M, Tanaka S, Tobiume M, Asaka M, Ohba Y. A novel FRET-based biosensor for the measurement of BCR-ABL activity and its response to drugs in living cells. Clin Cancer Res. 2010; 16:3964–3975. [PubMed: 20670950]

Nakashima N, Rose DW, Xiao S, Egawa K, Martin SS, Haruta T, Saltiel AR, Olefsky JM. The functional role of CrkII in actin cytoskeleton organization and mitogenesis. J Biol Chem. 1999; 274:3001–3008. [PubMed: 9915838]

Olcese L, Lang P, Vély F, Cambiaggi A, Marguet D, Bléry M, Hippen KL, Biassoni R, Moretta A, Moretta L, et al. Human and mouse killer-cell inhibitory receptors recruit PTP1C and PTPlD protein tyrosine phosphatases. J Immunol. 1996; 156:4531–4534. [PubMed: 8648092]

Peterson ME, Long EO. Inhibitory receptor signaling via tyrosine phosphorylation of the adaptor Crk. Immunity. 2008; 29:578–588. [PubMed: 18835194]

Ravetch JV, Lanier LL. Immune inhibitory receptors. Science. 2000; 290:84–89. [PubMed: 11021804]

Reedquist KA, Ross E, Koop EA, Wolthuis RM, Zwartkruis FJ, van Kooyk Y, Salmon M, Buckley CD, Bos JL. The small GTPase, Rap1, mediates CD31-induced integrin adhesion. J Cell Biol. 2000; 148:1151–1158. [PubMed: 10725328]

Riteau B, Barber DF, Long EO. Vav1 phosphorylation is induced by beta2 integrin engagement on natural killer cells upstream of actin cytoskeleton and lipid raft reorganization. J Exp Med. 2003; 198:469–474. [PubMed: 12885870]

Schleinitz N, March ME, Long EO. Recruitment of activation receptors at inhibitory NK cell immune synapses. PLoS One. 2008; 3:e3278. [PubMed: 18818767]

Segovis CM, Schoon RA, Dick CJ, Nacusi LP, Leibson PJ, Billadeau DD. PI3K links NKG2D signaling to a CrkL pathway involved in natural killer cell adhesion, polarity, and granule secretion. J Immunol. 2009; 182:6933–6942. [PubMed: 19454690]

Standeven LJ, Carlin LM, Borszcz P, Davis DM, Burshtyn DN. The actin cytoskeleton controls the efficiency of killer Ig-like receptor accumulation at inhibitory NK cell immune synapses. J Immunol. 2004; 173:5617–5625. [PubMed: 15494512]

Stebbins CC, Watzl C, Billadeau DD, Leibson PJ, Burshtyn DN, Long EO. Vav1 dephosphorylation by the tyrosine phosphatase SHP-1 as a mechanism for inhibition of cellular cytotoxicity. Mol Cell Biol. 2003; 23:6291–6299. [PubMed: 12917349]

ten Hoeve J, Morris C, Heisterkamp N, Groffen J. Isolation and chromosomal localization of CRKL, a human crk-like gene. Oncogene. 1993; 8:2469–2474. [PubMed: 8361759]

Tolar P, Sohn HW, Pierce SK. Viewing the antigen-induced initiation of B-cell activation in living cells. Immunol Rev. 2008; 221:64–76. [PubMed: 18275475]

Tybulewicz VL. Vav-family proteins in T-cell signalling. Curr Opin Immunol. 2005; 17:267–274. [PubMed: 15886116]

Varma R, Campi G, Yokosuka T, Saito T, Dustin ML. T cell receptor-proximal signals are sustained in peripheral microclusters and terminated in the central supramolecular activation cluster. Immunity. 2006; 25:117–127. [PubMed: 16860761]

Virgin HW, Wherry EJ, Ahmed R. Redefining chronic viral infection. Cell. 2009; 138:30–50. [PubMed: 19596234]

Vyas YM, Mehta KM, Morgan M, Maniar H, Butros L, Jung S, Burkhardt JK, Dupont B. Spatial organization of signal transduction molecules in the NK cell immune synapses during MHC class I-regulated noncytolytic and cytolytic interactions. J Immunol. 2001; 167:4358–4367. [PubMed: 11591760]

Yokoyama WM, Kim S. Licensing of natural killer cells by self-major histocompatibility complex class I. Immunol Rev. 2006; 214:143–154. [PubMed: 17100882]

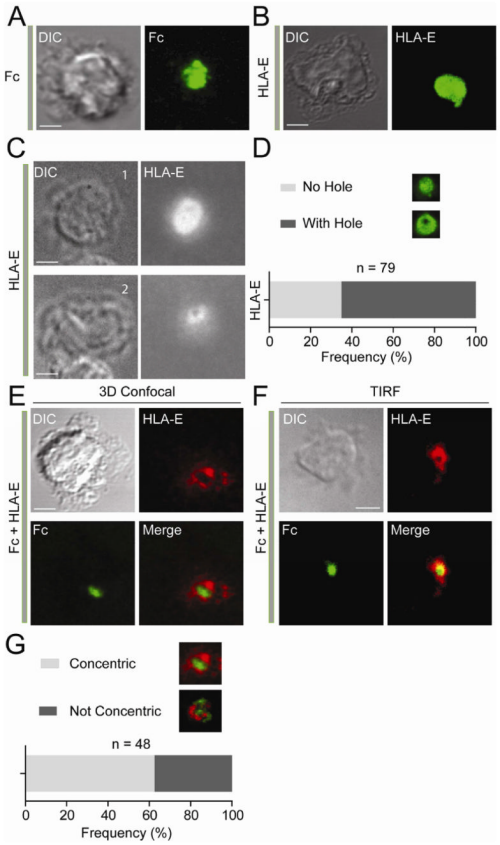

Figure 1. Inhibitory NK Cell Immunological Synapses Formed with IgG1 Fc and HLA-E

(A and B) Three-dimensional confocal images of fixed NK cells over lipid bilayers carrying Fc-Alexa Fluor 488 (A) and HLA-E-Alexa Fluor 488 (B). (C) TIRF image of two different fixed NK cells over a lipid bilayer carrying HLA-E-Alexa Fluor 568. Cell #1 shows HLA-E clustering without hole. Cell #2 shows HLA-E clustering with a central hole. The frequency of each type of clustering is shown in (D). (E) Three-dimensional confocal images of fixed NK cells over bilayers carrying HLA-E-Alexa Fluor 568 (Red) and Fc-Alexa Fluor 488 (Green). (F) TIRF image of a live NK cell over a bilayer carrying HLA-E-Alexa Fluor 568 (Red) and Fc-Alexa Fluor 488 (Green). (G) Frequency of organized, concentric synapses versus disorganized synapses. Scale bars are 3.0 μm. NK cells were fixed about 60 min after addition to bilayers. The images are representative of at least 100 cells for TIRF images and 48 cells for 3D confocal images in three independent experiments.

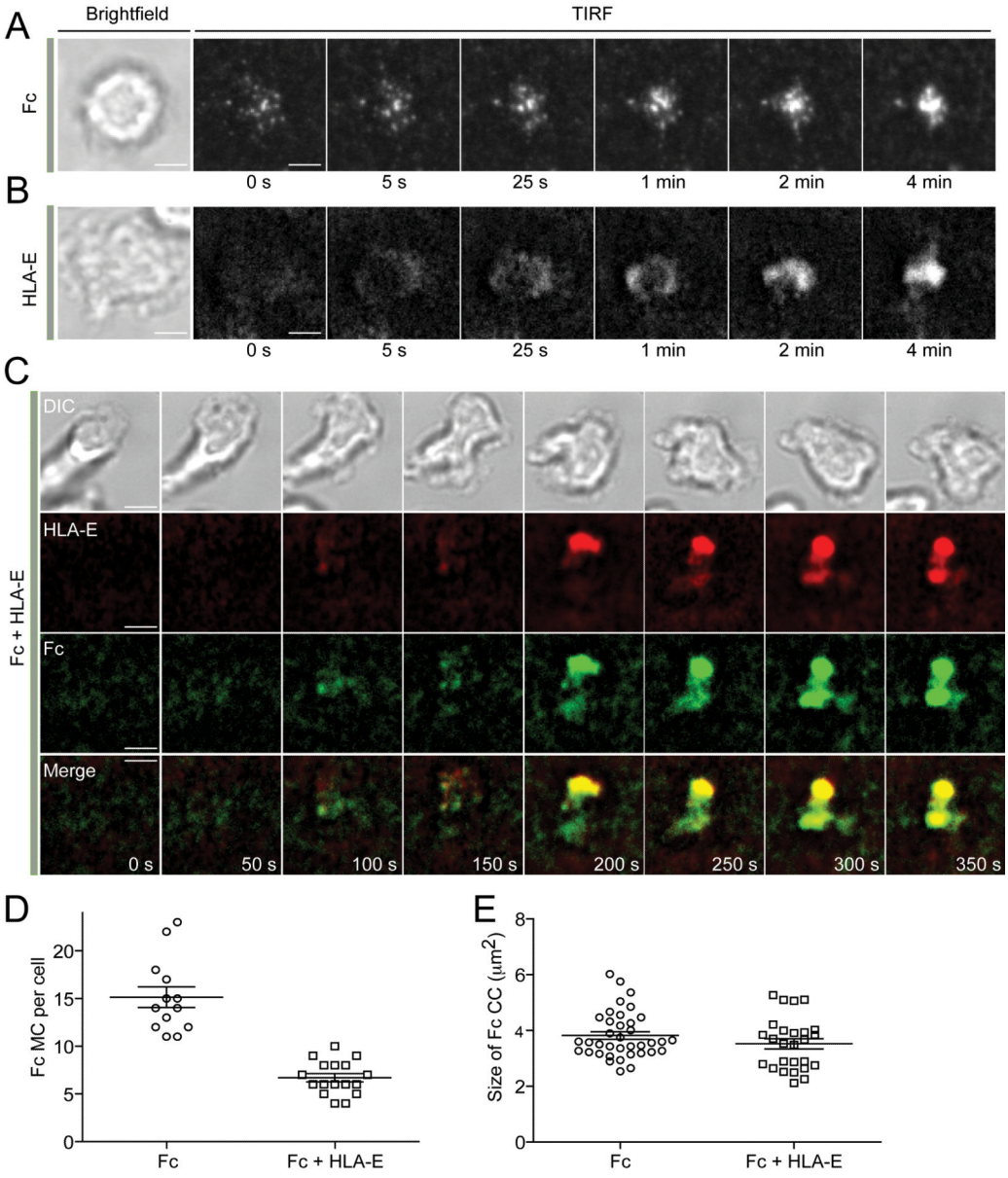

Figure 2. Live Imaging of Inhibitory NK Cell Immunological Synapses

(A and B) Live TIRF images of NK cells after addition to bilayers carrying either Fc-Alexa Fluor 568 (A) or HLA-E-Alexa Fluor 568 (B). (C) TIRF images of a live NK cell ~2 min after addition to a lipid bilayer carrying HLA-E-Alexa Fluor 568 (Red) and Fc-Alexa Fluor 488 (Green). (D) Number of peripheral Fc microcluster (MC) formed on Fc alone and on Fc with HLA-E (Fc + HLA-E). (E) The size of central clusters (CC) of Fc formed on Fc alone and on Fc with HLA-E (Fc + HLA-E). Scale bars represent 3.0 μm. Error bars indicate the standard error of the mean (SEM). The images are representative of at least 17 cells in two independent experiments.

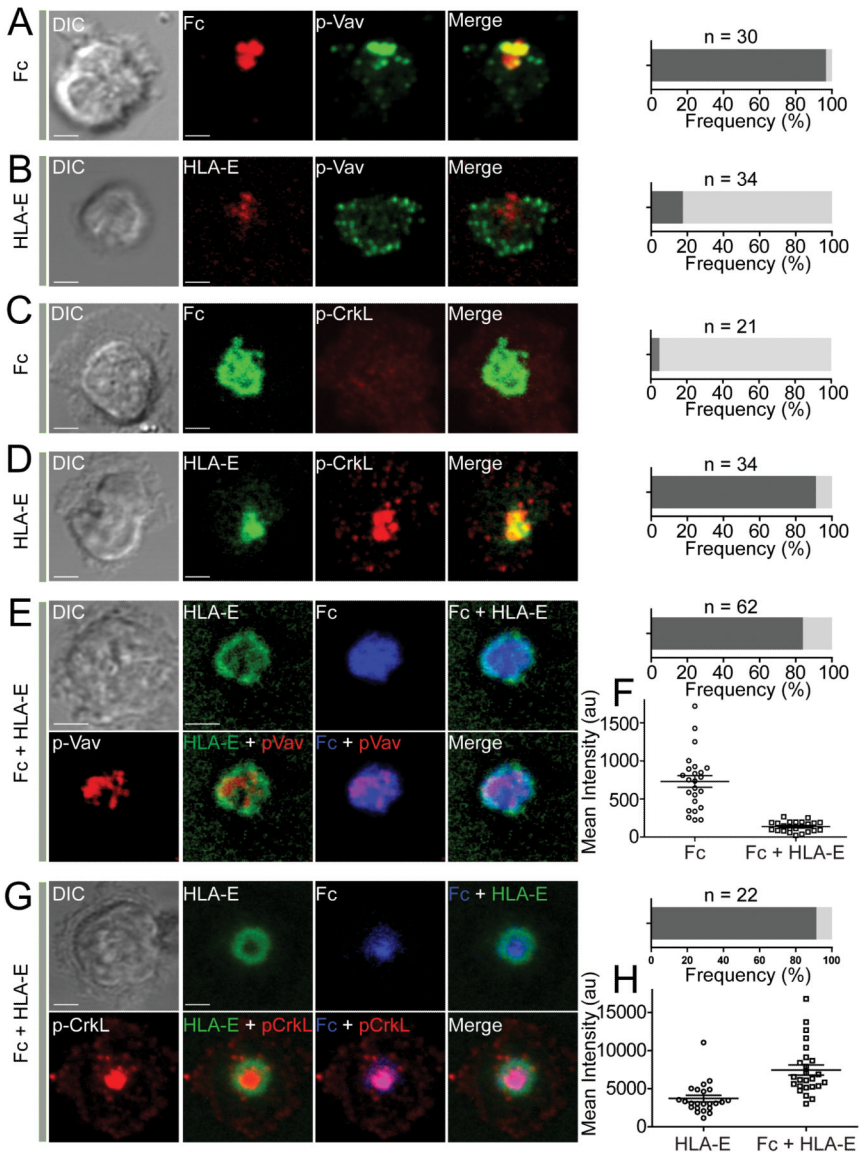

Figure 3. HLA-E Induces Central Accumulation of Phosphorylated Crk

(A and B) 3-D confocal images of NK cells on lipid bilayers carrying either Fc-Alexa Fluor 568 (A) or HLA-E-Alexa Fluor 568 (B). Fixed and permeabilized cells were incubated with Abs to pY174-Vav1 and with Alexa Fluor 488-conjugated secondary Ab. The frequency of cells showing overlapping Fc and p-Vav (A) or HLA-E and p-Vav (B) is indicated by dark shaded bars on the *right*. Cells with non-overlapping staining are indicated by light shaded bars. (C and D) 3-D confocal images of NK cells on lipid bilayers carrying either Fc-Alexa Fluor 488 (C) or HLA-E-Alexa Fluor 488 (D). Fixed and permeabilized cells were incubated with Abs to pY207-CrkL and with Alexa Fluor 568-conjugated secondary Ab. The frequency of cells showing overlapping Fc and p-CrkL (C) or HLA-E and p-CrkL (D) is indicated by dark shaded bars on the right. Cells with non-overlapping staining are indicated by light shaded bars. (E) 3-D confocal imaging of an NK cell on a lipid bilayer carrying Fc-Alexa Fluor 568 (Blue) and HLA-E-Alexa Fluor 488 (Green). pY174-Vav1 was stained as in (A) but with an Alexa Fluor 647-conjugated secondary Ab (Red). The dark shaded bar on the *right* indicates cells displaying phosphorylated Vav-1 at the center within a ring-like

distribution of HLA-E. The light shaded bar indicates cells with organized inhibitory synapses and without central pY174-Vav1. (F) The mean fluorescence intensity of phosphorylated Vav1 was determined for activating (Fc) and inhibitory (Fc + HLA-E) synapses by TIRF microscopy. (G) 3-D confocal imaging of an NK cell on a lipid bilayer carrying Fc-Alexa Fluor 568 (Blue) and HLA-E-Alexa Fluor 488 (Green). Phosphorylated CrkL was stained as in D (Red). The dark shaded bar on the *right* indicates cells with central accumulation of p-Crk within a ring-like distribution of HLA-E. The light shaded bar indicates cells with organized inhibitory synapses without central accumulation of p-Crk. (H) The mean fluorescence intensity of phosphorylated CrkL induced by HLA-E alone (HLA-E) or at inhibitory synapses (Fc + HLA-E) was determined by TIRF microscopy. Scale bars are 3.0 μm. Error bars indicate the standard error of the mean (SEM). Images were captured ~60 min after adding NK cells onto the bilayer. The images are representative of at least 20 cells in two independent experiments.

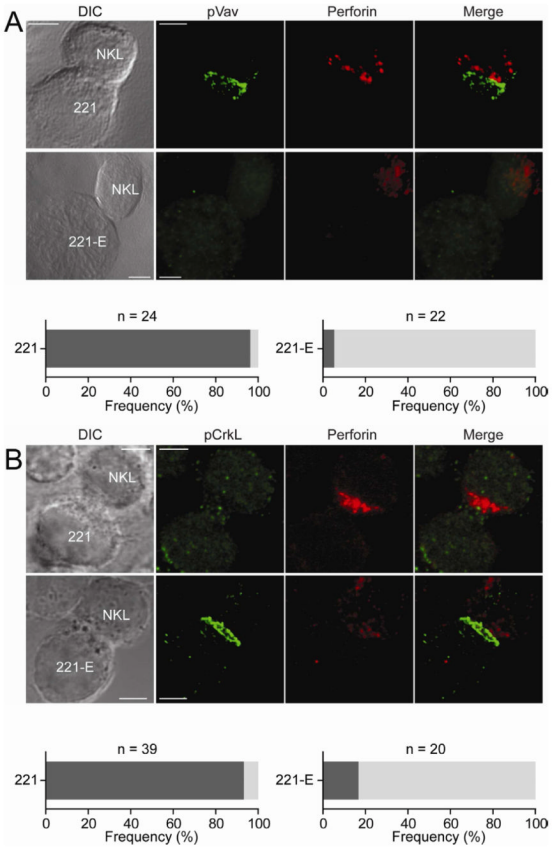

Figure 4. Phosphorylated Crk Accumulates at Inhibitory Synapses between NKL and 221-E Cells

NKL cells were conjugated with the HLA class I-negative human cell line 721.22l (221), and 221 cells expressing HLA-E (221-E) for 60 min. DIC images are shown on the *Left*. Confocal microscope z-series were obtained and projected serial confocal sections are shown. (A) Fixed and permeabilized cells were incubated with Abs to pY174-Vav1 followed by Alexa Fluor 488-conjugated secondary Abs (Green). Perforin was stained with a primary Ab followed by Alexa Fluor 647-conjugated secondary mAb (Red). Merged overlays are on the *Right*. For conjugates with 221 cells, the dark shaded bar indicates the frequency of cells displaying polarization of perforin and pVav-1. For conjugates with 221-E, the dark shaded bar indicates cells displaying polarization of p-Vav1, but not perforin; the light shaded bar indicates cells with neither perforin nor p-Vav1 polarization. (B) Fixed and permeabilized cells were incubated with Abs to pY207-CrkL followed by Alexa Fluor 488-conjugated secondary Abs (Green). Perforin was stained as in (A). For 221 conjugates, the dark shaded bar indicates cells displaying polarization of perforin and no p-CrkL. For 221-E conjugates, the dark shaded bar indicates cells displaying no perforin polarization and no p-CrkL; the light shaded bar indicates cells displaying polarization of p-CrkL, but not perforin. Scale bars are 2.0 μm. The images are representative of 20 cells in two independent experiments.

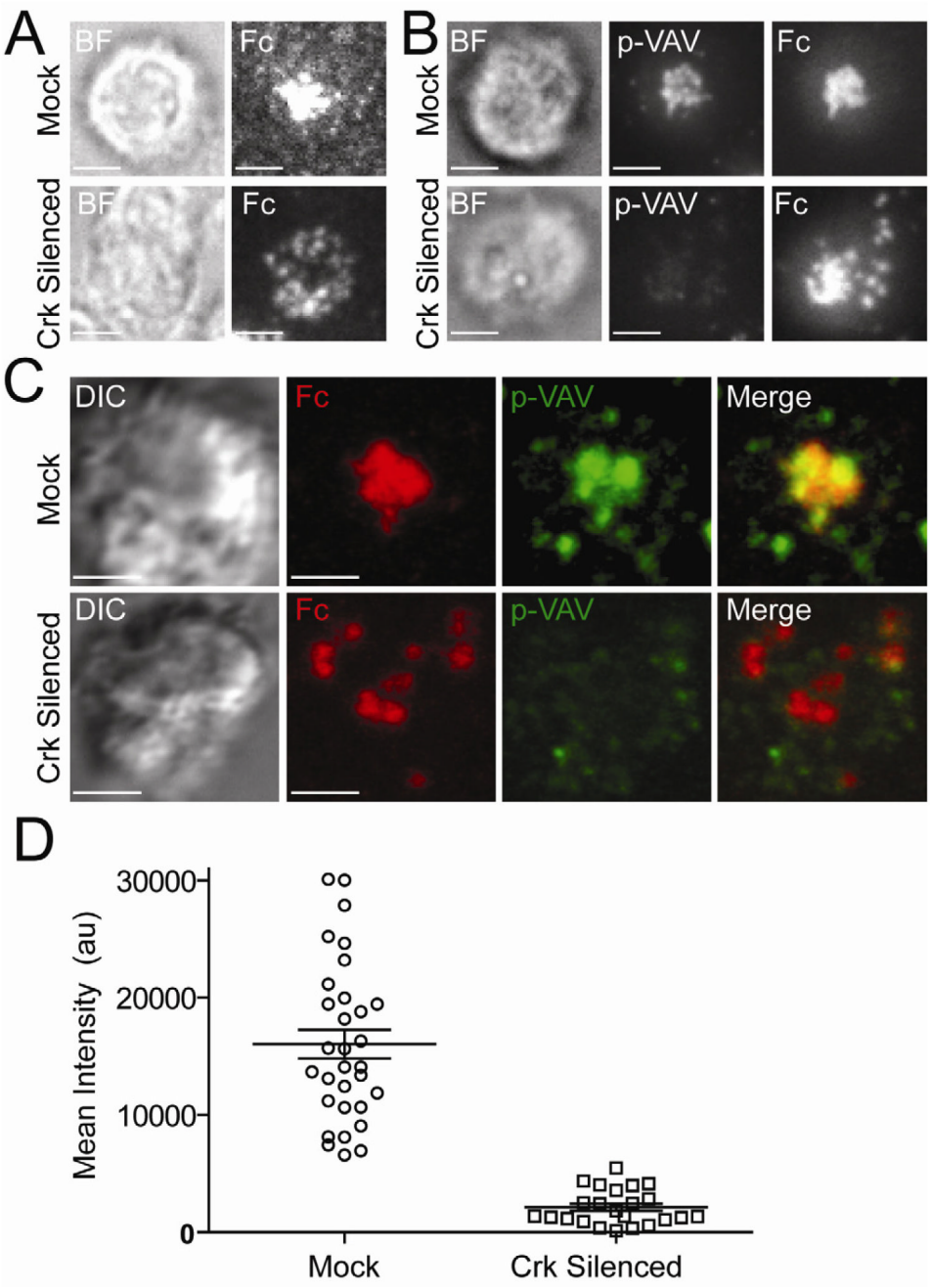

Figure 5. Crk Silencing Inhibits Fc Clustering and Vav1 Phosphorylation

(A–B) TIRF images of NK cells transfected with control siRNA (Mock) and siRNAs for CrkII and CrkL (Crk Silenced) incubated for 30 min on lipid bilayers carrying Fc-Alexa Fluor 568. Brightfield (BF) images are shown on the *Left*. (A) Live NK cells. (B) Fixed and permeabilized NK cells stained for pY174-Vav1 followed by Alexa Fluor 647 conjugated secondary Ab. Total CrkL was stained with primary Ab followed by Alexa Fluor 488-conjugated secondary Ab in order to select cells with strong silencing. (C) 3D confocal imaging of NK cells ~45 min after addition to a lipid bilayer carrying Fc-Alexa Fluor 568 (Red). Treatment with siRNA, and staining for pY174-Vav1 and CrkL was as in (A–B). (D) Mean intensity, in arbitrary units (au), of pY174-Vav1 in NK cells treated with control

siRNA (Mock) and Crk siRNAs (Crk silenced), incubated for 60 min on lipid bilayers carrying Fc, and imaged by TIRF. Scale bars are 3.0 μm. Error bars indicate the standard error of the mean (SEM). The images are representative of at least 23 cells in three independent experiments.

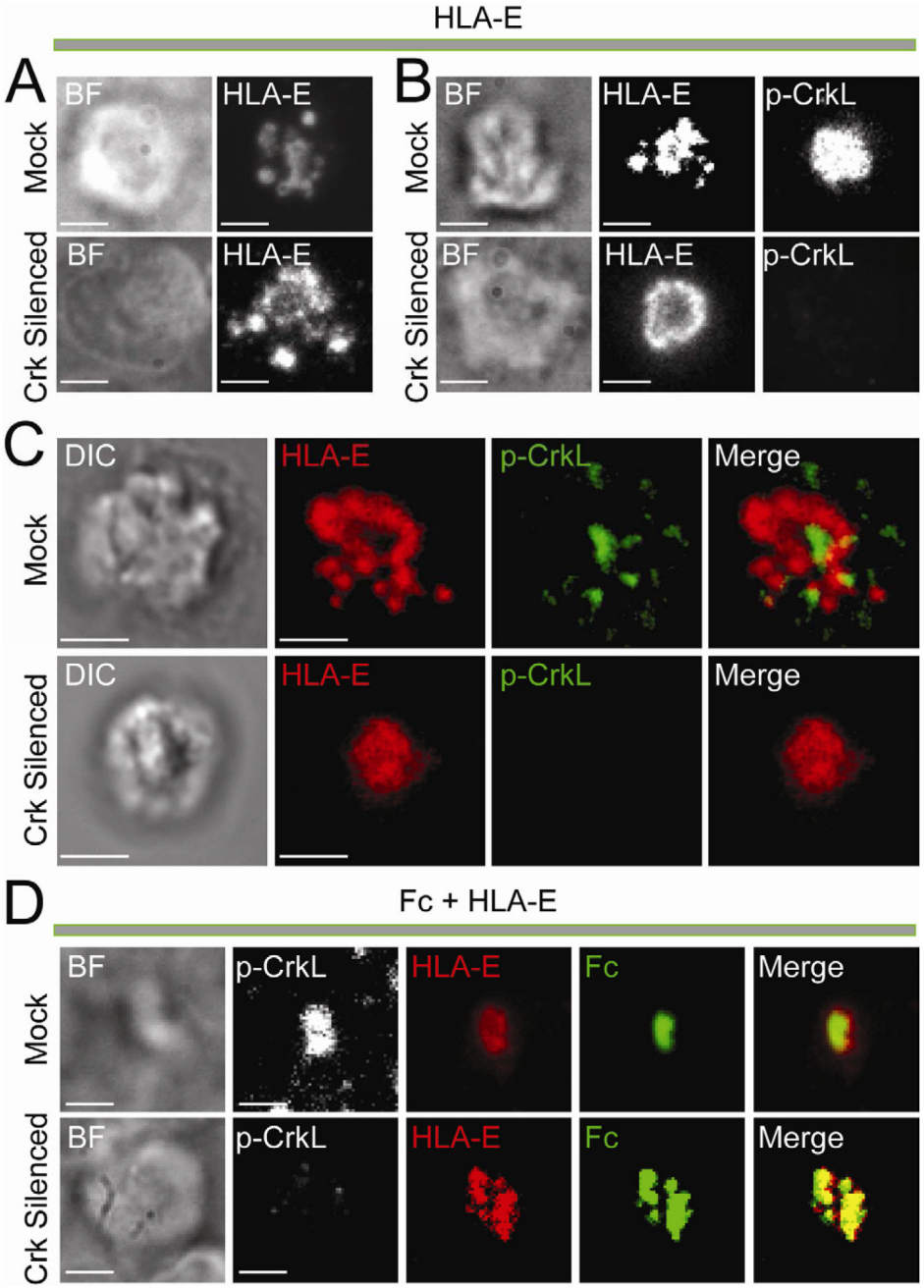

Figure 6. HLA-E Promotes Crk-Independent Central Clustering of Fc

(A–C) Images of NK cells transfected with control siRNA (Mock) and Crk siRNAs (Crk silenced) and incubated on lipid bilayers carrying HLA-E-Alexa Fluor 568. Brightfield (BF) images are shown on the *Left*. (A) TIRF images of live NK cells at 30 min. (B) TIRF images of NK cells fixed after 30 min and stained with pY207-CrkL primary Ab followed by Alexa Fluor-488-conjugated secondary Ab. (C) 3D confocal imaging of NK cells fixed ~60 min after addition to the lipid bilayer. Staining for pY207-CrkL (Green) was as in (B). (D) TIRF images of NK cells fixed ~50 min after addition to a lipid bilayer carrying Fc-Alexa Fluor 488 (Green) and HLA-E-Alexa Fluor 568 (Red), and stained for pY207-CrkL with primary Ab followed by Alexa Fluor 647-conjugated secondary Ab (White). Treatment with siRNAs

was as in (A–C). Scale bars are 3.0 μm. The images are representative of at least 100 cells in three independent experiments.

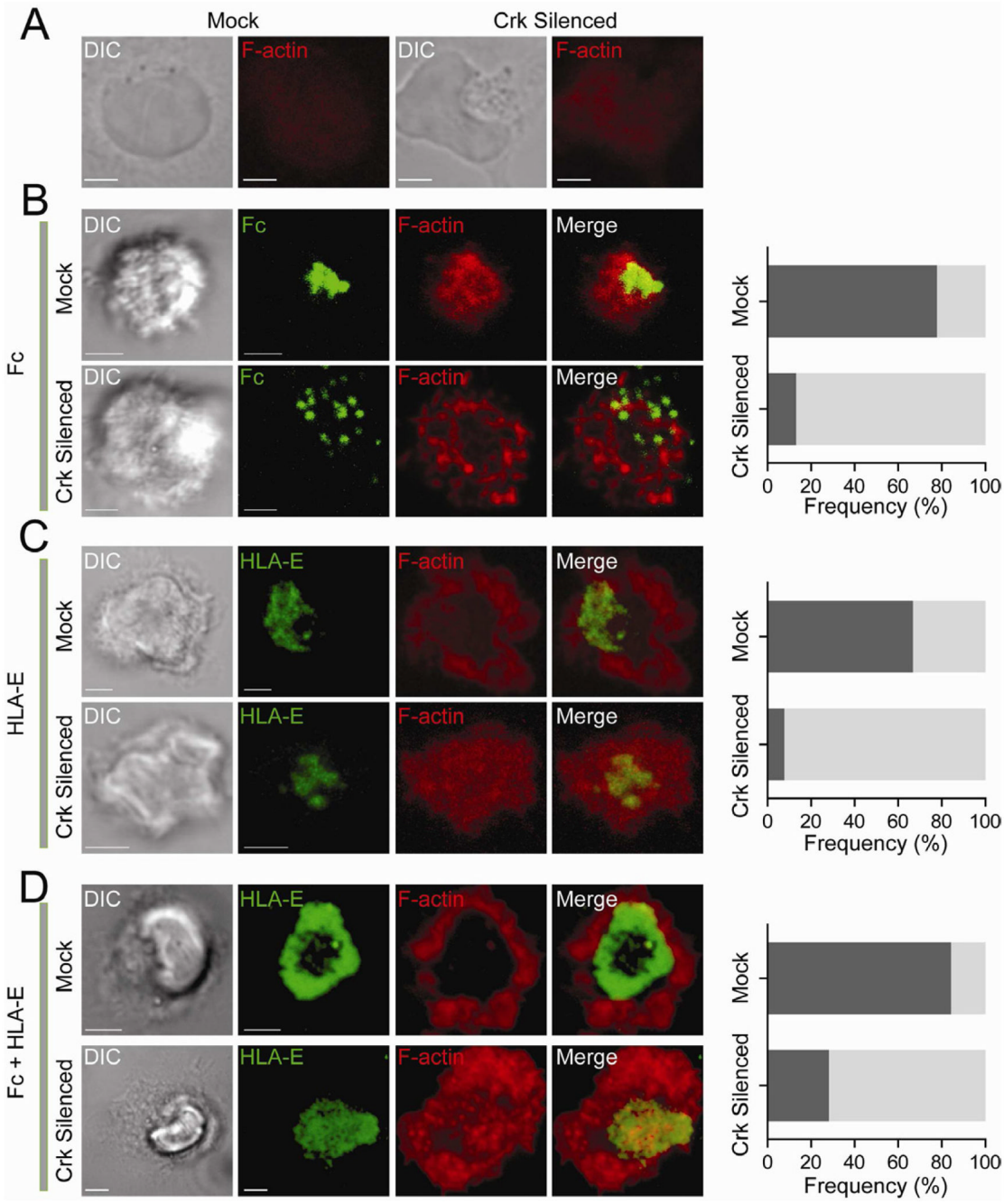

Figure 7. Crk Is Required for the HLA-E–Dependent Block in F-Actin Accumulation

Confocal z-series of NK cells transfected with control siRNA (Mock) and Crk siRNAs (Crk silenced) and stained for F-actin with phalloidin-Alexa Fluor 647. Total CrkL was stained with primary Ab followed by Alexa Fluor 488-conjugated secondary Ab in order to select cells with strong silencing. DIC images are shown on the *Left*. Scale bars are 3.0 μm. (A) NK cells on poly-L-lysine. (B) NK cells incubated for ~60 min on lipid bilayers carrying Fc-Alexa Fluor 568. Dark shaded bars represent the frequency of cells with F-actin accumulation toward the center. Light shaded bars represent cells with disorganized or dispersed F-actin. (C) NK cells incubated for ~60 min on lipid bilayers carrying HLA-E-Alexa Fluor 568. Dark shaded bars represent cells with a peripheral F-actin ring. Light

shaded bars represent cells with diffuse F-actin. (D) NK cells incubated for ~60 min on lipid bilayers carrying HLA-E-Alexa Fluor 568 and Fc. Dark shaded bars represent cells with a peripheral F-actin ring. Light shaded bars represent cells with disorganized F-actin. The images are representative of at least 20 cells in three independent experiments.